Lepton flavour universality test at the CERN NA62 experiment

Evgueni Goudzovski[a] on behalf of the NA62 collaboration

[a]School of Physics and Astronomy, University of Birmingham,
Edgbaston, Birmingham, B15 2TT, United Kingdom

A precision test of lepton universality by measurement of the ratio R_K of $K^+ \to e^+\nu$ to $K^+ \to \mu^+\nu$ decay rates was performed using a sample of 59963 $K^+ \to e^+\nu$ candidates with 8.8% background contamination collected by the CERN NA62 experiment. The result $R_K = (2.486 \pm 0.013) \times 10^{-5}$ is in agreement with the Standard Model expectation.

1. Introduction

Decays of pseudoscalar mesons to light leptons are suppressed in the Standard Model (SM) by angular momentum conservation. In particular, the SM width of $P^\pm \to l^\pm\nu$ decays (with $P = \pi, K, D_{(s)}, B$) is

$$\Gamma^{\rm SM} = \frac{G_F^2 M_P M_\ell^2}{8\pi}\left(1-\frac{M_\ell^2}{M_P^2}\right)^2 f_P^2 |V_{qq'}|^2,$$

where G_F is the Fermi constant, M_P and M_ℓ are meson and lepton masses, f_P is the decay constant, and $V_{qq'}$ is the corresponding CKM matrix element.

Within the two Higgs doublet models (2HDM of type II), including the minimal supersymmetric one, the charged Higgs boson ($H^\pm$) exchange induces a tree-level contribution to (semi)leptonic decays proportional to the Yukawa couplings of quarks and leptons [1]. In $P^\pm \to \ell^\pm\nu$, it can compete with the $W^\pm$ exchange due to the helicity suppression of the latter. At tree level, the $H^\pm$ exchange contribution is lepton flavour independent, and for $P = \pi, K, B$ leads to [2]

$$\frac{\Gamma(P^\pm \to \ell^\pm\nu)}{\Gamma^{\rm SM}(P^\pm \to \ell^\pm\nu)} = \left[1-\left(\frac{M_P}{M_H}\right)^2 \frac{\tan^2\beta}{1+\varepsilon_0\tan\beta}\right]^2.$$

Here M_H is the $H^\pm$ mass, $\tan\beta$ is the ratio of the two Higgs vacuum expectation values, and $\varepsilon_0 \approx 10^{-2}$ is an effective coupling.

A plausible choice of parameters $M_H = 500$ GeV/c^2, $\tan\beta = 40$ leads to $\sim 30\%$ relative suppression of $B^+ \to \ell^+\nu$ decays, and $\sim 0.3\%$ suppression of $K^+, D_s^+ \to \ell^+\nu$ decays with respect to their SM rates. However, searches for new physics in the decay rates are hindered by the uncertainties of their SM predictions. In particular, interpretation of the measurements of the ratio $\Gamma(K^+ \to \mu^+\nu)/\Gamma(K^+ \to \pi^0\mu^+\nu)$ in terms of constraints on $(M_H, \tan\beta)$ phase space is currently limited by lattice QCD uncertainties [3].

On the other hand, the ratio of kaon leptonic decay widths $R_K = \Gamma(K_{e2})/\Gamma(K_{\mu 2})$, where the notation $K_{\ell 2}$ is adopted for $K^+ \to \ell^+\nu$ decays, is sensitive to loop-induced lepton flavour violating (LFV) effects via the $H^\pm$ exchange [4]:

$$\Delta R_K/R_K^{\rm SM} \simeq \left(\frac{M_K}{M_H}\right)^4 \left(\frac{M_\tau}{M_e}\right)^2 |\Delta_R^{31}|^2 \tan^6\beta,$$

where the mixing parameter between the superpartners of the right-handed leptons $|\Delta_R^{31}|$ can reach $\sim 10^{-3}$. This can enhance R_K by $\mathcal{O}(1\%)$ relative without contradicting any presently known experimental constraints, including upper bounds on the LFV decays $\tau \to eX$ with $X = \eta, \gamma, \mu\mu$.

Unlike the individual $K_{\ell 2}$ decay widths, the ratio $R_K = \Gamma(K_{e2})/\Gamma(K_{\mu 2})$ is precisely predicted within the SM due to cancellation of hadronic uncertainties [5]:

$$R_K^{\rm SM} = \left(\frac{M_e}{M_\mu}\right)^2 \left(\frac{M_K^2-M_e^2}{M_K^2-M_\mu^2}\right)^2 (1+\delta R_{\rm QED}) = \\ = (2.477 \pm 0.001) \times 10^{-5},$$

where $\delta R_{\rm QED} = (-3.79 \pm 0.04)\%$ is an electromagnetic correction due to the internal bremsstrahlung (IB) process.

The sensitivity to LFV and the precision of the SM prediction make R_K an excellent probe of lepton universality. The current world average (based on final results only) $R_K^{\rm WA} = (2.490 \pm 0.030) \times 10^{-5}$ is dominated by a recent KLOE result [6]. A precise measurement of R_K based on a part (40%) of the data sample collected by the CERN NA62 experiment in 2007 is reported here. This is an update of an earlier result obtained with the same data sample [7].

2. Beam, detector and data taking

The NA48/2 experimental setup [8] has been used for the NA62 2007–08 data taking. Experimental conditions have been optimized for the $K_{e2}/K_{\mu 2}$ measurement. The beam line is designed to deliver simultaneous unseparated K^+ and K^- beams derived from the SPS 400 GeV/c primary protons. However, the muon sweeping system was optimized for the positive beam in 2007, and the sample used for the present analysis was collected with the K^+ beam only. Positively charged particles within a narrow momentum band of (74.0 ± 1.6) GeV/c are selected by an achromatic system of four dipole magnets with zero total deflection, pass through a muon sweeping system, and enter a fiducial decay volume contained in a 114 m long cylindrical vacuum tank.

With about 1.8×10^{12} primary protons incident on the target per SPS pulse of about 4.8 s duration, the secondary beam flux at the entrance to the decay volume is 2.5×10^7 particles per pulse, of which 5% are kaons (K^+). The fraction of beam kaons decaying in the vacuum tank at nominal momentum is 18%. The transverse size of the beam within the decay volume is $\delta x = \delta y = 7$ mm (rms), and its angular divergence is negligible.

Among the subdetectors located downstream the decay volume, a magnetic spectrometer, a plastic scintillator hodoscope (HOD) and a liquid krypton electromagnetic calorimeter (LKr) are principal for the measurement. The spectrometer, used to detect charged products of kaon decays, is composed of four drift chambers (DCHs) and a dipole magnet. The HOD producing fast trigger signals consists of two planes of strip-shaped counters. The LKr, used for particle identification and as a veto, is an almost homogeneous ionization chamber, $27X_0$ deep, segmented transversally into 13,248 cells (2×2 cm^2 each), and with no longitudinal segmentation. A beam pipe traversing the centres of the detectors allows undecayed beam particles and muons from decays of beam pions to continue their path in vacuum.

A minimum bias trigger configuration has been employed. The K_{e2} trigger condition consists of coincidence of hits in the two HOD planes (the Q_1 signal), loose lower and upper limits on DCH hit multiplicity (the 1-track signal), and LKr energy deposit ($E_{\rm LKr}$) of at least 10 GeV. The $K_{\mu 2}$ trigger condition requires a coincidence of the Q_1 and 1-track signals downscaled by a factor $D = 150$.

3. Measurement strategy, event selection

The analysis strategy is based on counting the numbers of reconstructed K_{e2} and $K_{\mu 2}$ candidates collected concurrently. Thus the analysis does not rely on the absolute beam flux measurement, and several systematic effects (e.g. due to charged track reconstruction and Q_1 trigger efficiencies, time-dependent effects) cancel at first order.

Due to the significant acceptance and background dependence, the measurement is performed independently in 10 bins of lepton momentum covering a range from 13 to 65 GeV/c. The first bin spans 7 GeV/c, while the others are 5 GeV/c wide. The selection conditions have been optimized separately in each momentum bin. The ratio R_K in each bin is computed as

$$R_K = \frac{1}{D} \cdot \frac{N(K_{e2}) - N_{\rm B}(K_{e2})}{N(K_{\mu 2}) - N_{\rm B}(K_{\mu 2})} \cdot \frac{A(K_{\mu 2})}{A(K_{e2})} \times \frac{f_\mu \times \epsilon(K_{\mu 2})}{f_e \times \epsilon(K_{e2})} \cdot \frac{1}{f_{\rm LKr}},$$

where $N(K_{\ell 2})$ are the numbers of selected $K_{\ell 2}$ candidates ($\ell = e, \mu$), $N_{\rm B}(K_{\ell 2})$ are the numbers of background events, $A(K_{\mu 2})/A(K_{e2})$ is the geometric acceptance correction, f_ℓ are the lepton identification efficiencies, $\epsilon(K_{\ell 2})$ are the trigger efficiencies, $f_{\rm LKr}$ is the global efficiency of the LKr

readout, and $D = 150$ is the $K_{\mu 2}$ trigger downscaling factor.

To evaluate the acceptance correction and the geometric parts of the acceptances for background processes, a detailed Monte Carlo (MC) simulation including beam line optics, full detector geometry and material description, magnetic fields, local inefficiencies of DCH wires, non-working LKr cells (0.8% of channels) and temporarily masked LKr cells is used. Particle identification, trigger and readout efficiencies are measured directly from data.

Charged particle tracks are reconstructed from hits and drift times in the spectrometer. Track momenta are evaluated using a detailed magnetic field map. Clusters of energy deposition in the LKr are found by looking at the maxima in the digitized pulses from individual cells in both space and time, and accumulating the energy within a radius of 11 cm. Shower energies are corrected for energy outside the cluster boundary, energy lost in non-working cells, and cluster energy sharing.

Due to the topological similarity of K_{e2} and $K_{\mu 2}$ decays, a large part of the selection is common for the two modes: (1) exactly one reconstructed particle of positive electric charge geometrically consistent with originating from a kaon decay is required; (2) extrapolated track impact points in the DCHs, HOD and LKr must be within their geometrical acceptances; (3) track momentum must be in the range (13; 65) GeV/c, where the lower limit assures the efficiency of the $E_{\rm LKr} > 10$ GeV trigger condition; (4) no LKr energy deposition clusters with energy $E > E_{\rm veto} = 2$ GeV and in time with the track are allowed unless they are consistent with being produced by the track via direct energy deposition or bremsstrahlung; (5) the reconstructed decay vertex longitudinal position must be within the nominal decay volume; (6) distance between the charged track and the nominal kaon beam axis must be below 3.5 cm.

The following two principal criteria are used to distinguish K_{e2} from $K_{\mu 2}$ decays. Kinematic identification is based on constraining the reconstructed squared missing mass in positron (muon) hypothesis $-M_1^2 < M^2_{\rm miss}(\ell) = (P_K - P_\ell)^2 < M_2^2$, where P_K and P_ℓ are the four-momenta of the

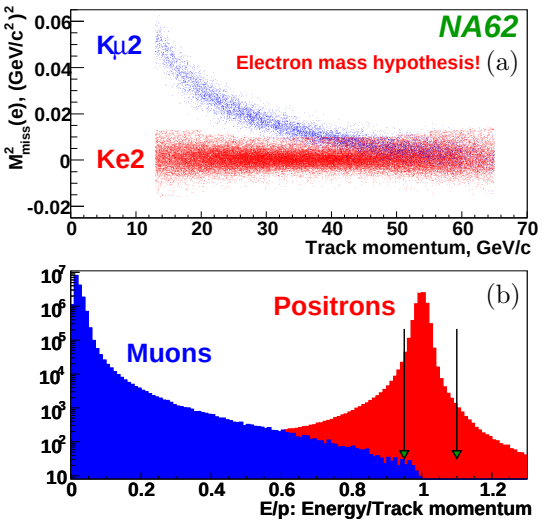

Figure 1. (a) $M^2_{\rm miss}(e)$ vs lepton momentum for reconstructed K_{e2} and $K_{\mu 2}$ decays; (b) E/p spectra of positrons and muons.

kaon (defined as the average one monitored with $K^+ \to \pi^+\pi^+\pi^-$ decays) and the lepton (under the e^+ or μ^+ mass hypothesis). The limits M_1^2 and M_2^2 have been optimized taking into account the resolution and backgrounds, and vary among lepton momentum bins in the ranges (0.013; 0.016) and (0.010; 0.014) (GeV/c^2)^2, respectively. Lepton identification is based on the ratio E/p of track energy deposition in the LKr to its momentum measured by the spectrometer. Tracks with $(E/p)_{\rm min} < E/p < 1.1$, where $(E/p)_{\rm min} = 0.95$ for $p > 25$ GeV/c and $(E/p)_{\rm min} = 0.9$ otherwise, are identified as positrons. Tracks with $E/p < 0.85$ are identified as muons.

4. Backgrounds

Kinematic separation of K_{e2} from $K_{\mu 2}$ decays is achievable at low lepton momentum only ($p <$ 30 GeV/c), as shown in Fig. 1a. At high lepton momentum, the $K_{\mu 2}$ decay with the muon misidentified as positron ($E/p > 0.95$, as shown in Fig. 1b) due to 'catastrophic' bremsstrahlung in or in front of the LKr is the largest background source. In order to measure the mis-identification probability $P_{\mu e}$, a muon sample free from the typical $\sim 10^{-4}$ positron contamination due to $\mu \to e$ decays has been collected: a $9.2X_0$ thick lead (Pb)

wall covering $\sim 20\%$ of the geometric acceptance was installed in front of the LKr during a period of data taking. The positron component in a sample of muon candidates consistent with originating from $K_{\mu 2}$ decays, traversing the Pb wall, with $p > 30$ GeV/c and $E/p > 0.95$ is suppressed to a negligible level ($\sim 10^{-8}$) by energy losses in the Pb wall.

However, the muon passage through the Pb wall affects the measured $P_{\mu e}^{\rm Pb}$ via two principal effects: 1) ionization energy loss in Pb decreases $P_{\mu e}$ and dominates at low momentum; 2) bremsstrahlung in Pb increases $P_{\mu e}$ and dominates at high momentum. To evaluate the corresponding correction factor $f_{\rm Pb} = P_{\mu e}/P_{\mu e}^{\rm Pb}$, a dedicated Geant4 based [9] MC simulation of muon propagation downstream the spectrometer involving all electromagnetic processes, including muon bremsstrahlung [10], has been developed. The relative systematic uncertainties on $P_{\mu e}$ and $P_{\mu e}^{\rm Pb}$ obtained by simulation are estimated to be 10%, mainly due to the simulation of cluster geometry and calibration (measured and simulated $P_{\mu e}^{\rm Pb}$ are shown in Fig. 2). However, the error affecting their ratio is significantly smaller ($\delta f_{\rm Pb}/f_{\rm Pb} = 2\%$) due to partial cancellation of uncertainties.

The $K_{\mu 2}$ background contamination has been computed to be (6.10±0.22)% using the measured $P_{\mu e}^{\rm Pb}$ corrected by the simulated $f_{\rm Pb}$, and correcting for the correlation between the reconstructed $M^2_{\rm miss}(e)$ and E/p. The uncertainty comes from the limited size of the data sample used to measure $P_{\mu e}^{\rm Pb}$ (0.16%), the uncertainty $\delta f_{\rm Pb}$ (0.12%), and model-dependence of the $M^2_{\rm miss}(e)$ vs E/p correlation (0.08%).

The $K_{\mu 2}$ decay also contributes to background via the $\mu \to e$ decay in flight. Energetic forward daughter positrons compatible with K_{e2} kinematics and topology are suppressed by muon polarization effects [11]. Radiative corrections to the muon decay [12] lead to a further $\sim 10\%$ relative background suppression. The background contamination has been estimated to be $(0.27 \pm 0.04)\%$.

The structure-dependent (SD) $K^+ \to e^+\nu\gamma$ process [13], not suppressed by angular momentum conservation (more specifically, its SD$^+$ component corresponding to positive photon helicity), represents a significant background source. A recent measurement of the $K^+ \to e^+\nu\gamma$ (SD$^+$) differential decay rate [6] has been used to evaluate the background contamination to be $(1.15 \pm 0.17)\%$. The dominant uncertainty comes from the uncertainty on the rate of $K^+ \to e^+\nu\gamma$ (SD$^+$) decay, which has been increased by a factor of 3 with respect to that reported in [6], as suggested by a stability check of R_K with respect to a variation of the $E_{\rm veto}$ limit.

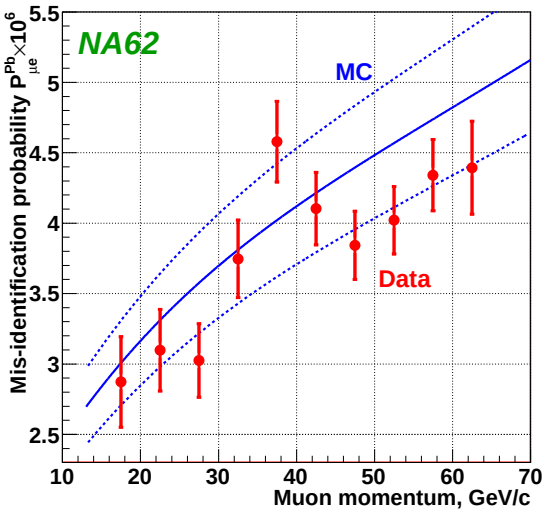

Figure 2. Muon mis-identification probability with the Pb wall installed $P_{\mu e}^{\rm Pb}$ for $(E/p)_{\rm min} = 0.95$ vs momentum: measurement (markers with error bars); simulation with its uncertainty (solid and dashed lines).

The beam halo background is induced by halo muons undergoing $\mu \to e$ decays in the vacuum tank, or being mis-identified as positrons. It has been measured directly by reconstructing the K^+_{e2} candidates from a K^- data sample collected with the K^+ beam (but not its halo) blocked, and a special data sample collected with both beams blocked. The control sample is normalized to the data in the region $-0.3 < M^2_{\rm miss}(\mu) < -0.1$ (GeV/c^2)^2 populated predominantly by beam halo events. The 'cross-talk' probability to reconstruct a K^+_{e2} candidate due to a K^- decay with e^+ emission ($K^- \to \pi^0_D \ell^- \nu$, $K^- \to \pi^-\pi^0_D$, $K^- \to \ell^-\nu e^+ e^-$, where π^0_D denotes the π^0 Dalitz decay $\pi^0 \to \gamma e^+ e^-$) is at

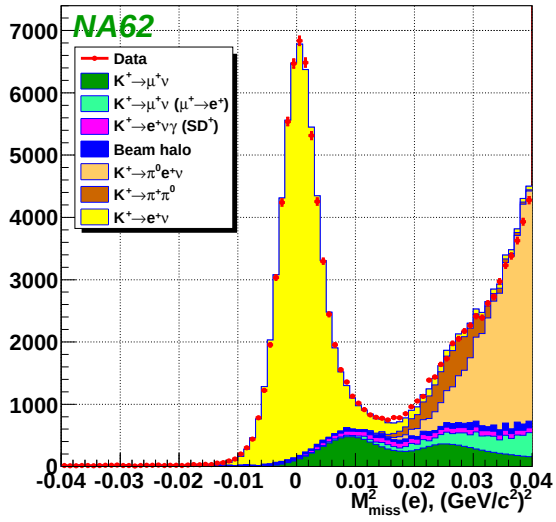

Figure 3. Reconstructed squared missing mass $M^2_{\rm miss}(e)$ distribution of the K_{e2} candidates compared with the sum of normalised MC signal and background components.

Table 1
Summary of backgrounds in the K_{e2} sample.

Source	$N_B/N(K_{e2})$
$K_{\mu 2}$	$(6.10 \pm 0.22)\%$
$K_{\mu 2}$ $(\mu \to e)$	$(0.27 \pm 0.04)\%$
$K_{e2\gamma}$ (SD^+)	$(1.15 \pm 0.17)\%$
Beam halo	$(1.14 \pm 0.06)\%$
K_{e3}	$(0.06 \pm 0.01)\%$
$K_{2\pi}$	$(0.06 \pm 0.01)\%$
Total background	$(8.78 \pm 0.29)\%$

the level of $\sim 10^{-4}$ and is taken into account. The halo background contamination has been estimated to be $(1.14 \pm 0.06)\%$, where the uncertainty comes from the limited size of the control sample and the uncertainty of its normalization. The beam halo is the only significant background source in the $K_{\mu 2}$ sample, measured to be $(0.38 \pm 0.01)\%$ with the same technique.

The number of $K_{\ell 2}$ candidates is $N(K_{e2}) = 59,963$ (about four times the statistics collected by KLOE) and $N(K_{\mu 2}) = 1.803 \times 10^7$. The $M^2_{\rm miss}(e)$ distributions of data events and backgrounds are presented in Fig. 3; backgrounds in the K_{e2} sample integrated over lepton momentum are summarized in Table 1.

5. Systematic uncertainties

The ratio of geometric acceptances $A(K_{\mu 2})/A(K_{e2})$ in each lepton momentum bin has been evaluated with a MC simulation. The radiative $K^+ \to e^+\nu\gamma$ (IB) process is simulated following [13] with higher order corrections according to [14,15]. Lepton tracking inefficiency due to interactions with the spectrometer material is included into the acceptance correction, and its simulation has been validated with the data. The main sources of systematic uncertainty of the acceptance correction are the limited knowledge of beam profile and divergence, accidental activity, and the simulation of soft radiative photons. A separate uncertainty has been assigned due to the limited precision of the DCH alignment.

A sample of $\sim 4 \times 10^7$ positrons selected kinematically from $K^+ \to \pi^0 e^+ \nu$ decays collected concurrently with the main $K_{\ell 2}$ data set is used to calibrate the energy response of each LKr cell, and to study f_e with respect to local position and time stability (in the kinematically limited momentum range $p < 50$ GeV/c). A sample of electrons and positrons from the $4{\times}10^6$ $K_L \to \pi^\pm e^\mp \nu$ decays collected during a special short (15h) run with a broad momentum band K^0_L beam allows the determination of f_e in the whole analysis momentum range. The measurements of f_e have been performed in bins of lepton momentum; separate measurements have been performed for several identified groups of LKr cells with higher local inefficiencies. The inefficiency averaged over the K_{e2} sample is $1 - f_e = (0.73 \pm 0.05)\%$, where the uncertainty takes into account the statistical precision and the small differences between K^+ and K^0_L measurements.

The efficiency of the Q_1 trigger condition has been measured using $K_{\mu 2}$ events triggered with a special control LKr signal: integrated over the $K_{\mu 2}$ sample, it is $(1.4 \pm 0.1)\%$. Owing to its geometric uniformity, and the similarity of the K_{e2} and $K_{\mu 2}$ distributions over the HOD plane, it mostly cancels between the K_{e2} and $K_{\mu 2}$ samples, and the residual systematic bias on R_K is negligible. The inefficiency of the 1-track trigger for $K_{\ell 2}$ modes is negligible. The trigger efficiency

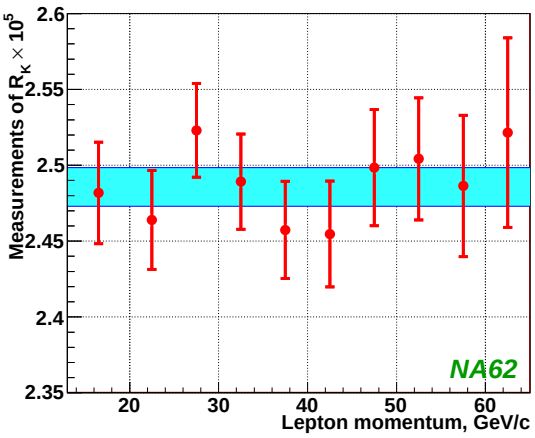

Figure 4. Measurements of R_K in lepton momentum bins, and the averaged R_K (indicated by a band). The uncertainties in momentum bins are partially correlated, and include statistical and systematic contributions.

Table 2
Summary of the uncertainties on R_K.

Source	$\delta R_K \times 10^5$
Statistical	0.011
$K_{\mu 2}$ background	0.005
$K^+ \to e^+\nu\gamma$ (SD$^+$) background	0.004
Beam halo background	0.001
Acceptance correction	0.002
Spectrometer alignment	0.001
Positron identification	0.001
1-track trigger efficiency	0.002

correction $\epsilon(K_{\mu 2})/\epsilon(K_{e2})$ is determined by the efficiency $\epsilon(E_{\rm LKr})$ of the LKr energy deposit trigger signal $E_{\rm LKr} > 10$ GeV, which has been measured to be $1 - \epsilon(E_{\rm LKr}) = (0.41 \pm 0.05)\%$ in the first lepton momentum bin of (13; 20) GeV/c, and to be negligible in the other momentum bins. The corresponding uncertainty on R_K is negligible.

Energetic photons not reconstructed in the LKr may initiate showers by interacting in the DCH or beam pipe material, which causes the DCH hit multiplicities to exceed the limits allowed by the 1-track trigger condition. This suppresses the $K^+ \to e^+\nu\gamma$ (SD$^+$) background by about 10% relative (varying over the positron momentum). Evaluation of the 1-track inefficiency for $K^+ \to e^+\nu\gamma$ (SD$^+$) partially relies on simulation; its uncertainty has been propagated into R_K.

The global LKr readout inefficiency has been measured using an independent readout system to be $1 - f_{\rm LKr} = (0.20 \pm 0.03)\%$ and stable in time.

6. Result and conclusions

The independent measurements of R_K in the 10 lepton momentum bins and the average over the bins are displayed in Fig. 4. Extensive stability checks in bins of kinematic variables, against variation of selection criteria and analysis procedures have been performed. The uncertainties of the combined result are summarized in Table 2. The result is

$$\begin{aligned} R_K &= (2.486 \pm 0.011_{\rm stat.} \pm 0.008_{\rm syst.}) \times 10^{-5} \\ &= (2.486 \pm 0.013) \times 10^{-5}. \end{aligned}$$

This is the most precise measurement to date; it is consistent with the SM expectation.

REFERENCES

1. W.-S. Hou, Phys. Rev. D48 (1993) 2342.
2. G. Isidori and P. Paradisi, Phys. Lett. B639 (2006) 499.
3. M. Antonelli *et al.*, arXiv:1005.2323.
4. A. Masiero, P. Paradisi and R. Petronzio, Phys. Rev. D74 (2006) 011701.
5. V. Cirigliano and I. Rosell, Phys. Rev. Lett. 99 (2007) 231801.
6. F. Ambrosino *et al.*, Eur. Phys. J. C64 (2009) 627. Erratum-ibid. C65 (2010) 703.
7. E. Goudzovski, arXiv:1005.1192.
8. V. Fanti *et al.*, Nucl. Instrum. Methods A574 (2007) 433.
9. S. Agostinelli *et al.*, Nucl. Instrum. Methods A506 (2003) 250.
10. S.R. Kelner, R.P. Kokoulin and A.A. Petrukhin, Phys. Atom. Nucl. 60 (1997) 576.
11. L. Michel, Proc. Phys. Soc. A63 (1950) 514.
12. A. Arbuzov, A. Czarnecki and A. Gaponenko, Phys. Rev. D65 (2002) 113006.
13. J. Bijnens, G. Ecker and J. Gasser, Nucl. Phys. B396 (1993) 81.
14. S. Weinberg, Phys. Rev. 140 (1965) B516.
15. C. Gatti, Eur. Phys. J. C45 (2006) 417.